Energy & Environmental Science

ROYAL SOCIETY OF CHEMISTRY

PERSPECTIVE

View Article Online
View Journal | View Issue

Cite this: *Energy Environ. Sci.*, 2025, **18**, 10036

Computationally accelerated discovery of mixed metal compounds for chemical looping combustion and beyond

Kunran Yang and Fanxing Li *

Received 7th May 2025,
Accepted 14th October 2025

DOI: 10.1039/d5ee02521d

rsc.li/ees

Compared to their monometallic counterparts, mixed metal compounds, such as mixed metal oxides and nitrides, are highly versatile in their compositional, structural, redox, and surface properties. This versatility unlocks exciting opportunities for applications in clean energy conversion and sustainable chemical production. However, efficiently identifying optimal compositions remains a significant challenge due to the vast and complex material design space. This perspective discusses how high-throughput computational and data science tools are transforming the rational design of mixed metal compounds for chemical looping applications beyond combustion. The specific applications covered include chemical looping air separation, redox-based CO_2 and water splitting, NH_3 synthesis, and redox-activated CO_2 sorbents, among others. We aim to illustrate how high-throughput density functional theory (DFT) calculations, combined with machine learning and experimental validation, have accelerated material screening and optimization, enabling the efficient exploration of vast compound families. Finally, we discuss future trends aimed at improving the efficiency and accuracy of chemical looping carrier discovery.

Broader context

The global push toward carbon neutrality necessitates transformative technologies that can sustainably produce energy and chemicals while minimizing CO_2 emissions. Chemical looping processes offer an elegant solution by integrating redox-mediated reactions with inherent separation, enabling efficient energy conversion and chemical production. However, the discovery of suitable redox-active materials, particularly mixed metal compounds with tailored thermodynamic and surface properties, has remained a bottleneck due to the vast material design space. This work addresses this challenge by highlighting how computational screening and machine learning can accelerate the identification of optimal oxygen and nitrogen carriers for applications ranging from combustion and air separation to ammonia synthesis and CO_2 capture. Beyond enabling cleaner energy systems, these approaches promise to transform materials discovery by reducing experimental trial-and-error, guiding the design of new multifunctional materials, and laying the foundation for autonomous research platforms. By illustrating the synergy between computation, data science, and experimental validation, this perspective outlines a scalable and generalizable framework for rapid development of redox materials. These advancements are crucial for decarbonizing power and industrial sectors—major contributors to greenhouse gas emissions—and ensuring a more sustainable future.

1. Introduction

The chemical looping (CL) strategy, which makes use of cyclic reactions facilitated by a carrier or reaction medium, offers an excellent opportunity to integrate energy and/or chemical conversion with feedstock or product separation, leading to more sustainable processes. Over the past few decades, various applications for chemical looping have been explored. Examples include chemical looping combustion,[1–5] carbonate looping,[6–9] air separation,[10–12] solar thermal CO_2 and/or water splitting,[13–19] ammonia synthesis,[20–22] and selective oxidation or reduction for the production of chemicals,[23–29] to name a few. A large fraction of the aforementioned chemical looping applications relies on the redox reactions of a metal oxide-based oxygen carrier to facilitate the cyclic reaction. As such, oxygen carrier performance plays a critical role in the technical feasibility and economic attractiveness of many CL processes investigated to date. Nitrides and imides, on the other hand, have shown promise as nitrogen carriers for chemical looping ammonia synthesis.[30–32] Despite extensive research efforts related to the development of these carriers, their design and optimization are still mostly empirical based. Meanwhile, many recent studies have pointed to the excellent potential of mixed metal compounds when compared

Department of Chemical and Bimolecular Engineering, North Carolina State University, Raleigh, NC, USA. E-mail: fli5@ncsu.edu

to their monometallic counterparts.[33,34] As a result, the corresponding material design space has been substantially expanded, with infinite potential options for material compositions. Given that materials synthesis and evaluation guided by heuristics can be tedious and time-consuming, computational tools that can efficiently and accurately identify promising carrier compositions out of a large material design space are highly desirable.

Herein, we review recent advancements in the accelerated development of mixed metal compounds for chemical looping applications, leveraging high-throughput computational models and machine learning tools. The discussion begins with computationally assisted high-throughput development of oxygen carriers and their applications, followed by nitrogen carrier design and selection for ammonia synthesis. We then explore multifunctional oxygen and CO_2 carriers and their roles in CO_2 sorption-enhanced reforming and gasification. Finally, we provide perspectives on future research directions in this field.

2. Recent advances in mixed metal compound development

2.1. High-throughput development of oxygen carriers

2.1.1. Chemical looping combustion and chemical looping air separation. Simplified schematics of chemical looping combustion (CLC) and its variant, chemical looping air separation (CLAS), are shown in Fig. 1. CLC operates through two main steps for energy generation with integrated CO_2 capture: first, metal oxide carriers serve as oxidants to completely combust a carbonaceous feedstock, such as methane, coal, or biomass, producing a concentrated CO_2 stream after steam condensation.[23,35–43] Second, these reduced metal oxides are regenerated through exposure to the air. From a thermodynamic standpoint, the metal oxide carriers must maintain a favorable Gibbs free energy change (ΔG) to enable both the fuel oxidation and air regeneration steps, *i.e.*, the oxygen carrier reduction potential needs to be high enough for fuel combustion, while the subsequent re-oxidation with air must also be spontaneous. The primary concept behind CLC lies in its ability to separate oxygen from air *in situ* while indirectly oxidizing carbon-based fuels. As such, CLAS is a natural extension of CLC where a separated O_2 stream is the target product (Fig. 1b).[44–57] Oxygen carrier selection for CLAS is more restrictive thermodynamically than that for CLC since the oxide should spontaneously release gaseous oxygen under vacuum or steam purge (*i.e.* higher equilibrium P_{O_2}), while still being re-oxidizable by the air.

Inherent to their operating principles, the redox properties of oxygen carriers are crucial to all chemical looping processes involving lattice oxygen release and replenishment. However, systematic, bottom-up strategies for effectively designing oxygen carriers are still lacking. The inherent complexity of redox reactions, which extend well beyond the interaction between reactant molecules and often poorly defined oxide surfaces, makes it difficult to design redox oxides using first principles. This is particularly the case in the context of chemical looping catalysis, an emerging area receiving increased attention.[58–60] In such applications, oxides' surface catalytic properties play a major role in determining the overall reaction performance, in addition to the redox properties of the oxygen carriers.[61–66]

Although expecting an *ab initio* or DFT model to fully capture all aspects of oxygen carrier design is impractical, modern computational and data science tools, combined with relatively simple selection criteria, can greatly reduce the experimental workload in screening and developing oxygen carriers. As a starting point, it is rather straightforward to begin with the underlying thermodynamic requirements that drive the envisioned chemical looping reactions, as illustrated in Fig. 1. As early as 2017, Lau *et al.* screened over 5500 compounds from the Materials Project database to identify materials with suitable thermodynamic properties for redox based O_2 separation and chemical looping combustion, as well as their resistance toward carbonation.[67] Through a systematic screening

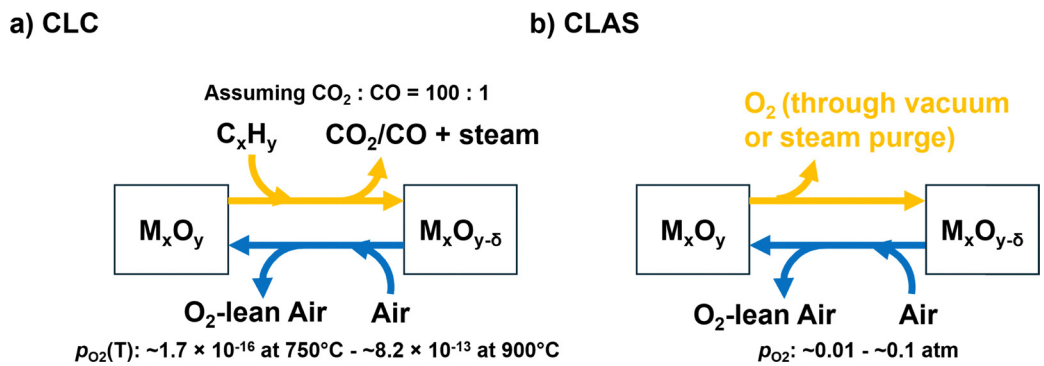

Fig. 1 Schematic illustration of (a) chemical looping combustion (CLC) and (b) CL air separation (CLAS) and thermodynamic criteria for the redox potential of the oxide expressed in terms of equilibrium P_{O_2}. For CLC, this value is calculated assuming a CO_2 : CO ratio of 100 : 1; the equilibrium P_{O_2} as a function of temperature can be approximated by $P_{O_2,eq} = 10^4 e^{(20.86-67885/T)}$ within the general temperature range of interest. The equation was obtained by calculating the P_{O_2} values that would lead to an equilibrium CO_2/CO ratio of 100 : 1 within a temperature range of 750 °C–900 °C based on the CO_2 thermolysis reaction ($2CO_2 \rightarrow 2CO + O_2$). The ΔG values of the CO_2 thermolysis reaction as a function of temperature (T) were calculated using the HSC Chemistry software.

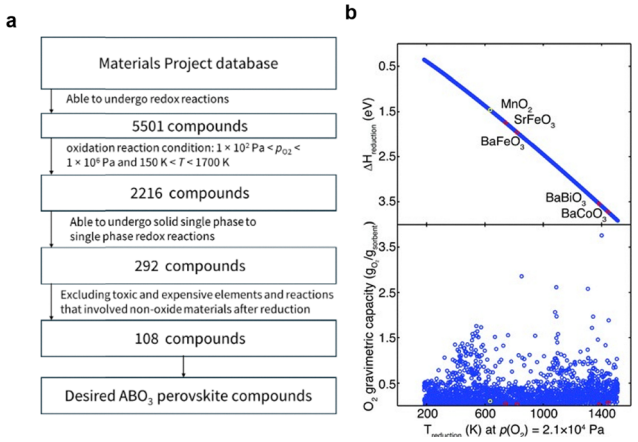

Fig. 2 (a) Screening workflow by Lau *et al.*,[67] plotted based on the description in the manuscript and SI data; (b) overview of the key results from screening the Materials Project database for compounds that undergo redox reactions.[67] The predicted reduction temperature at P_{O_2} = 2.1 × 10^4 Pa for each reaction is plotted against $\Delta H_{reduction}$ (upper panel) and O_2 gravimetric capacity (lower panel). (b) is adapted from ref. 67 with permission from the Royal Society of Chemistry, copyright 2017.

methodology (Fig. 2a), which considers the oxides' redox properties, equilibrium oxygen partial pressure, capability of single-phase redox reactions, and cost and toxicity, more than 100 promising perovskite oxides were identified, with $SrFeO_{3-\delta}$ emerging as the most promising candidate for chemical looping with oxygen uncoupling and CLAS at intermediate temperatures (< 823 K). Experimental validation showed that $SrFeO_{3-\delta}$ had excellent cycling stability and resistance to carbonation when synthesized as a pure phase, though impurities like $Sr_3Fe_2O_7$ led to unwanted carbonation reactions. The screening also revealed broader insights into stabilizing metal oxides within different structural frameworks to optimize their redox properties. It is interesting to note that a few compounds identified by this study (or those with similar compositions) were the subject of further experimental investigations, showing promising results.[68–73] This highlights the usefulness of the screening method built upon readily available computational databases.

Although the Materials Project database is highly useful, the accuracy of thermodynamic parameters for some oxide compounds of interest is limited. Wang *et al.* developed a systematic workflow (Fig. 3a), in conjunction with high-throughput DFT calculations, to select perovskite oxides with a general formula of $Sr_xA_{1-x}Fe_yB_{1-y}O_{3-\delta}$ (A = Ca, K, Y, Ba, La, Sm; B = Ti, Ni, Mn,

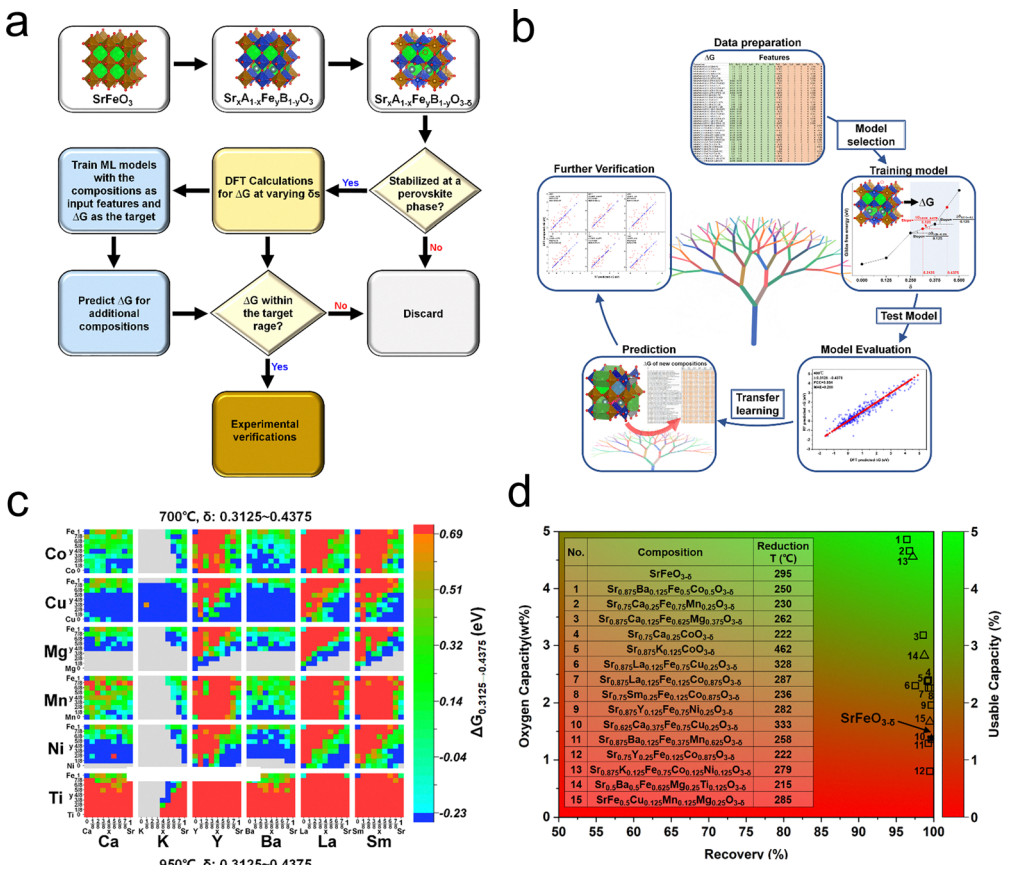

Fig. 3 High-throughput materials screening and experimental validation.[74] (a) DFT model construction, high-throughput calculations, and materials screening. (b) ML steps for the training, evaluation, and prediction of perovskite datasets. Heatmap of the screened candidates for (c) CLAS at 700 °C within the δ range of 0.3125–0.4375. (d) Experimental oxygen capacity, recovery, and usable capacity of the samples tested for CLAS. Squares and circles represent DFT- and ML-predicted samples, respectively.[74] This figure is adapted from ref. 74 with permission from the Royal Society of Chemistry, copyright 2021.

Mg, Cu, Co) for CLAS applications.[74] A cubic $SrFeO_{3-\delta}$ parent structure was chosen due to its high symmetry and ease of simulation. The DFT simulation covered more than two thousand distinct cation compositions. These results were then used to develop a machine learning model to predict the redox properties of over 200 000 perovskite oxides with a general composition of $Sr_x(A/A')_{1-x}Fe_y(B/B')_{1-y}O_{3-\delta}$. Fig. 3a summarizes the generalized simulation workflow, whereas Fig. 3b illustrates the machine learning (ML) procedure. The DFT simulations, which can predict the enthalpy and entropy changes related to oxygen vacancy creation at varying, discretized vacancy concentration levels, can project the equilibrium oxygen chemical potential (or equivalently oxygen partial pressure) as a function of perovskite oxide composition and its vacancy concentration level. As such, by comparing the predicted oxygen chemical potential ranges with the desirable ranges for CLAS, potentially suitable perovskite oxide compositions can be determined. The DFT simulation results can then be used to train the ML model to significantly expand the material design space with higher computational efficiency.

Of the 113 CLAS materials predicted by DFT (Fig. 3c), 11 compositions with similar structures have been validated in prior experimental studies and have shown outstanding performance. Building on these predictions, the authors prepared and experimentally evaluated 12 new compositions based on DFT predictions, along with 3 materials identified through machine learning (ML) models. All the 15 samples were assessed using a standardized experimental procedure, with $SrFeO_3$ serving as the reference material. As illustrated in Fig. 3d, a substantial portion of the computationally predicted materials demonstrated satisfactory CLAS performance: 13 of the 15 experimentally tested samples outperformed $SrFeO_3$ and 10 exhibited more than a 50% increase in oxygen capacity compared to $SrFeO_3$. Notably, some compositions, such as $Sr_{0.875}K_{0.125}Fe_{0.75}Co_{0.125}Ni_{0.125}O_{3-\delta}$, represent new discoveries without direct counterparts in the existing literature. These unique compositions would have been unlikely to emerge using traditional heuristic or empirical approaches, underscoring the transformative potential of the high-throughput methodology. Despite its effectiveness in identifying promising oxygen carrier compositions, the computational strategy developed in this study is nevertheless subjected to limitations due to the compromise between computational accuracy and efficiency, considering the complexity of perovskite oxides. As such, a number of simplifying assumptions were used in carrying out this study, as detailed in the manuscript.[74]

Duan and co-workers also adopted a high-throughput DFT screening approach to identify promising $SrFeO_{3-\delta}$-based perovskite materials for chemical looping, in particular CLAS and chemical looping with oxygen uncoupling.[69] They evaluated more than 1100 perovskite compositions by considering various dopant conditions and substitution patterns and calculated the oxygen vacancy formation energies (with an incremental $\Delta\delta$ of 0.0625) and Gibbs free energies of the candidate structures across a temperature range of 298–1200 K. These DFT results were then used to train various ML models, with the best-performing model (ALL-KNN) achieving an R^2 of 0.95 and an RMSE of 37 kJ mol^{-1} on test data. This ML model enabled rapid prediction of Gibbs free energies for new compositions, facilitating the identification of promising oxygen carrier materials. The authors validated their computational predictions through thermogravimetric analysis of oxygen storage capacity and O_2-temperature-programmed desorption. Their approach identified known high-performance materials (*e.g.*, $Sr_{1-x}Ca_xFe_{1-y}Ni_yO_{3-\delta}$) and predicted a new potential system ($Sr_{1-x}Ba_xFe_{1-y}Cu_yO_{3-\delta}$).

Singstock *et al.*[75] screened 13 763 compounds from the Materials Project database to identify suitable materials for the CLC and CL sulfur oxidation (CLSO) process. A systematic 5-step workflow was adopted (Fig. 2), considering the material stability, thermodynamic feasibility, and reaction performance. In terms of CLC, they highlighted 13 promising materials combining high oxygen storage capacity with low cost. They also demonstrated the method's broader applicability by using it to discover materials for the SO_2 production process, identifying 12 viable sulfate/sulfide pairs. Related to sulfur-based chemical looping, Tolstova *et al.* reported a high-throughput computational screening approach, again using Materials Project database, to identify promising materials for chemical looping elemental H_2S decomposition.[76]

Although the studies discussed above can greatly accelerate the development of oxygen carriers, these thermodynamic-based predictions can have limited utility when the carrier performance is kinetically limited. Moreover, formation of metastable phases and side reactions can also affect the usefulness of the thermodynamic-based parameters, which are typically calculated based on idealized overall reactions. Moreover, computational simulations face their own challenges, particularly when the structures undergo significant lattice and symmetry changes after heteroatom doping. It is also difficult to model arbitrary doping concentrations and accurately describe the energetics and local structures of defect formation and clustering. Additionally, various DFT parameters, including hybrid functionals, Hubbard *U* values, van der Waals interactions, and spin momentum, require careful calibration and validation before implementing high-throughput workflows, increasing both complexity and computational cost. These limitations highlight the notable gap between experimental results and computational predictions, ultimately affecting the accuracy of high-throughput calculations.

2.1.2. CO_2 or water-splitting. In this section, we first discuss chemical looping CO_2 and water splitting facilitated by methane partial oxidation, which is also known as chemical looping dry reforming of methane (CLDRM) or steam-methane reforming (CLSMR). The mechanism is shown in Fig. 4a. It is noted that the reaction scheme of CLDRM is different from that of traditional thermochemical CO_2 or water splitting, where no carbon-based fuels are involved in the reduction step. The workflow shown in Fig. 3 computationally predicts the redox properties and equilibrium oxygen chemical potentials of over 200 000 perovskite oxides. Using these data, oxygen carrier materials suitable for chemical looping CO_2 or water-splitting coupled with methane reforming were identified (Fig. 4a).

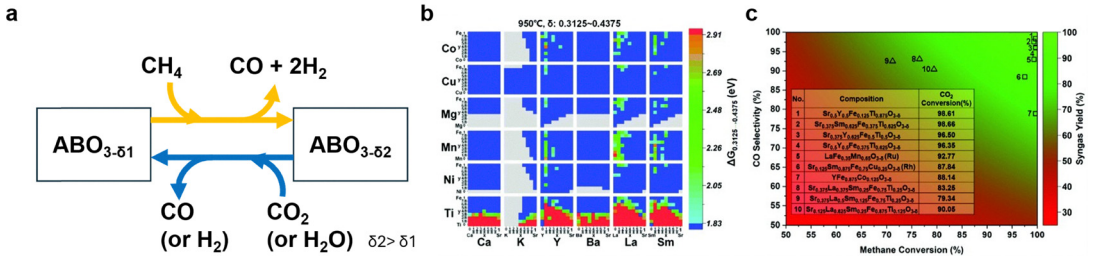

Fig. 4 (a) Scheme for chemical looping CO_2 or water-splitting on $ABO_{3-\delta}$ perovskite oxide structures. (b) A heatmap of the screened promising candidates for CL CO_2/H_2O splitting at 950 °C within the δ range of 0.3125–0.4375. (c) Experimental syngas yield and CO_2 conversion of the samples tested for CL CO_2 splitting. Squares and circles represent the DFT- and ML-predicted samples, respectively. (b) and (c) are adapted from ref. 74 with permission from the Royal Society of Chemistry, copyright 2021.

In this process, the oxygen carrier is first reduced by methane to produce a syngas product suitable for Fischer–Tropsch or methanol synthesis. This is followed by CO_2 or water splitting to generate CO or H_2. Similar to the findings in CLAS, the DFT prediction of suitable CLDRM materials (Fig. 4b) was largely validated by experimental results (Fig. 4c). 85 materials were predicted by DFT, and 4 of them have similar compositions and demonstrated excellent activity.[77,78] Of the ten samples the authors prepared and evaluated, all 7 samples predicted by DFT achieved over 80% syngas yield and more than 85% CO_2 conversion, while all three samples predicted by machine learning achieved over 70% syngas yield and more than 80% CO_2 conversion. It is noted that perovskite materials show promise for achieving higher lattice oxygen capacities than $CeO_{2-\delta}$ due to their structural flexibility and tunable composition. While many newly discovered materials may not immediately surpass established benchmarks, recent studies have demonstrated the applicability of computationally discovered materials under industrially relevant conditions and their potential for scale-up,[70] providing valuable insights for rational materials design and optimization.

In addition to methane-assisted CO_2 and water splitting processes, solar-thermal-driven water and CO_2 splitting can also benefit from high-throughput computational screening approaches. Emery *et al.* conducted a comprehensive DFT study of 5329 perovskite (ABO_3) compounds[79] to identify promising candidates for thermochemical water splitting. Their two-step screening process evaluated both thermodynamic stability and oxygen vacancy formation energies within specific ranges (2.5–5.0 eV per atom) suitable for water splitting applications. They identified 139 stable perovskites with favorable properties, including several previously unexplored materials like $CeCoO_3$ and $BiVO_3$. The researchers also demonstrated that traditional geometric criteria for perovskite stability (such as tolerance factors) are necessary but insufficient predictors of actual stability and performance.

2.1.3. Thermochemical energy storage. Besides CLAS and CLDRM, the high-throughput screening combined with DFT calculations on $SrFeO_{3-\delta}$-based perovskites can be readily adopted to design materials for thermochemical energy storage (TCES).[73,80] A typical TCES scheme is shown in Fig. 5. In this case, the material selection criteria focus on identifying

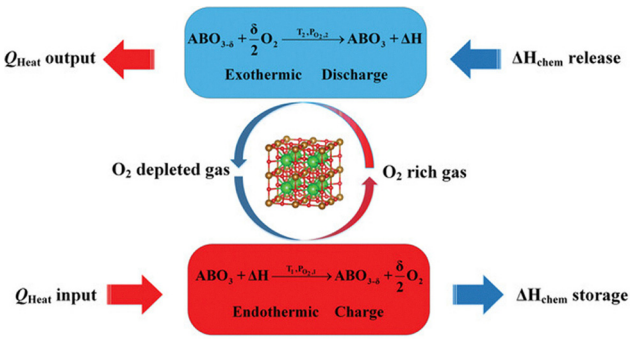

Fig. 5 The typical operating scheme of perovskite-based TCES. This figure is adapted from ref. 73 with permission from Wiley-VCH GmbH, copyright 2023.

materials with near-zero ΔG (feasible for releasing and replenishing gaseous oxygen) but high ΔH within desirable temperature and pressure swing windows (*e.g.* 400–800 °C, 0.01–0.2 atm). Based on DFT predictions, 61 promising TCES candidates were identified, with 45 materials featuring pure perovskite phases that underwent detailed evaluation. The experimental findings confirmed the high-throughput approach's effectiveness in determining the oxygen capacity and oxidation enthalpy of perovskite oxides. Many of the screened materials showed excellent performance under practical operating conditions: $Sr_{0.875}Ba_{0.125}FeO_{3-\delta}$ achieved a chemical energy storage density of 85 kJ kg^{-1} calculated from the ABO_3 structure in an isobaric environment with air between 400 °C and 800 °C, while $Sr_{0.125}Ca_{0.875}Fe_{0.25}Mn_{0.75}O_{3-\delta}$ demonstrated an energy density of 157 kJ kg^{-1}, ABO_3 between 400 °C at 0.2 atm and 1100 °C at 0.01 atm of O_2 (see Fig. 6). Integration of the experimental findings has in turn facilitated the development of an improved set of optimization criteria (Fig. 6c).

2.2. Nitrogen carriers

Besides mixed oxides, high-throughput screening for chemical looping materials can also be applied to identify nitrogen carriers in the context of chemical looping ammonia synthesis, as illustrated in Fig. 7a. Musgrave and colleagues screened 1148 metal nitride/metal oxide pairs by combining data from the Materials Project with a statistically learned descriptor for

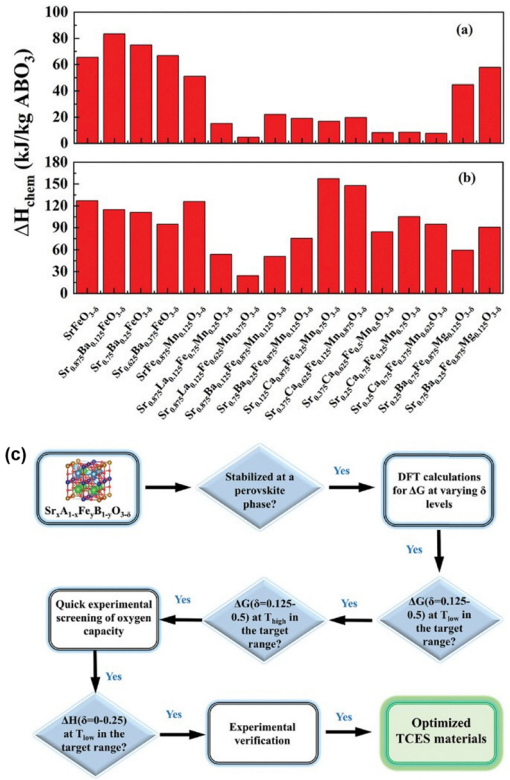

Fig. 6 (a) Thermochemical energy storage density of the screened materials between 400 °C/0.2 atm O_2 and 800 °C/0.2 atm O_2; (b) energy density between 400 °C/0.2 atm O_2 and 1100 °C/0.01 atm; (c) improved workflow based on experimental findings for high-throughput combinatorial screening of perovskite oxides for TCES. This figure is adapted from ref. 73 with permission from Wiley-VCH GmbH, copyright 2023.

temperature-dependent Gibbs energies.[30] They retrieved formation enthalpies for binary nitrides and oxides with <20 atoms per formula unit, excluding unstable compounds like azides and peroxides. Using their descriptor model and Gibbs energy minimization calculations, they assessed the thermodynamic viability of each reaction step in the solar thermochemical ammonia synthesis (STAS) cycle. They identified promising new materials based on B, V, Fe, and Ce and discovered that only 5 out of 1148 pairs exhibited yields >0.01 mol NH_3 per cycle (likely on a per mole of carrier basis) across all required reactions. When considering excess hydrogen feed to shift equilibrium, additional promising candidates based on Cr, Mo, Mn and W emerged. The reaction system and the Gibbs energy distribution are shown in Fig. 7. This work highlighted that the metal must bind nitrogen with a suitable strength. The proposed volcano relationship between oxide and nitride formation energies explains why finding viable materials for the complete cycle is challenging.

Similar to the aforementioned work, Hu and co-workers used the Materials Project database and screened 2515 nitride materials, evaluating their equilibrium nitrogen pressures and nitrogen exchange capacities.[32] This screening work identified 111 nitrides that can theoretically achieve sufficiently high ammonia yields to compete with the Haber–Bosch process. However, the uncertainties associated with these materials' thermodynamic properties make it difficult to confidently identify viable materials. A related study on thermochemical ammonia synthesis by Steinfeld's group also used materials' property data from the Materials Project database for screening nitrides.[81] When compared to experimental literature data, the predicted performance often differs significantly from experimental results. The authors conclude that improvements in both theoretical predictions and experimental validation are necessary to effectively identify suitable nitrogen carriers for chemical looping NH_3 synthesis.

Using machine learning (ML) methods and ML-driven interatomic potentials offers an interesting approach to generating additional thermodynamic data. Fan *et al.* conducted a computational screening of 1699 bicationic redox pairs for chemical looping ammonia synthesis.[31] They employed several machine learning approaches, including a Gibbs energy descriptor for thermodynamic predictions, the BOWSR algorithm for structure optimization, and MEGNet for formation energy calculations. They expanded the chemical space for metal hydride chemical looping by generating over 500 000 hypothetical compounds through elemental substitution. Their analysis revealed that three-step H_2O-CL showed the most promise, particularly when combining alkali/alkaline earth metals with transition metals. Such a process offers stronger thermodynamic driving forces compared to the H_2O-CL process between a metal oxide and nitride redox pair (M_aO_b/M_cN_d), and the H_2-CL process between two nitrides ($M_\alpha N_\beta/M_\alpha N_\gamma$). Notably, they introduced a new metric (λ) to evaluate "cooperative enhancement" between bicationic compounds and their simpler monocationic counterparts, finding that only about 17% of bicationic pairs showed genuine cooperative benefits. This challenges the assumption that more complex materials automatically perform better. Several promising new material combinations were identified, especially those containing Ni/Mn/Mo paired with alkali/alkaline earth metals.[21,82] For example, Gao *et al.* reported that NH_3 can be produced *via* a two-step chemical looping process mediated by the BaH_2/BaNH pair and Ni (for kinetic acceleration) at 100 °C and atmospheric pressure.[16]

While computational screening approaches have provided valuable insights into potential nitrogen carriers for chemical looping applications, their practical impact remains limited. High-throughput computational studies face challenges, including uncertainties in calculated thermodynamic properties, difficulties in modeling complex reaction mechanisms, and limited validation against experimental data. This explains the relatively low number of viable candidates identified despite screening thousands of materials. Nevertheless, this remains an active research area with complementary approaches being pursued. Experimental studies focusing on systematic testing of selected material families, such as alkali and alkaline earth metal imides,[21] provide crucial validation data, while more detailed and targeted computational investigations can greatly improve prediction accuracy.[83] These parallel efforts are potentially able to bridge the gap between theoretical predictions and experimental performance.

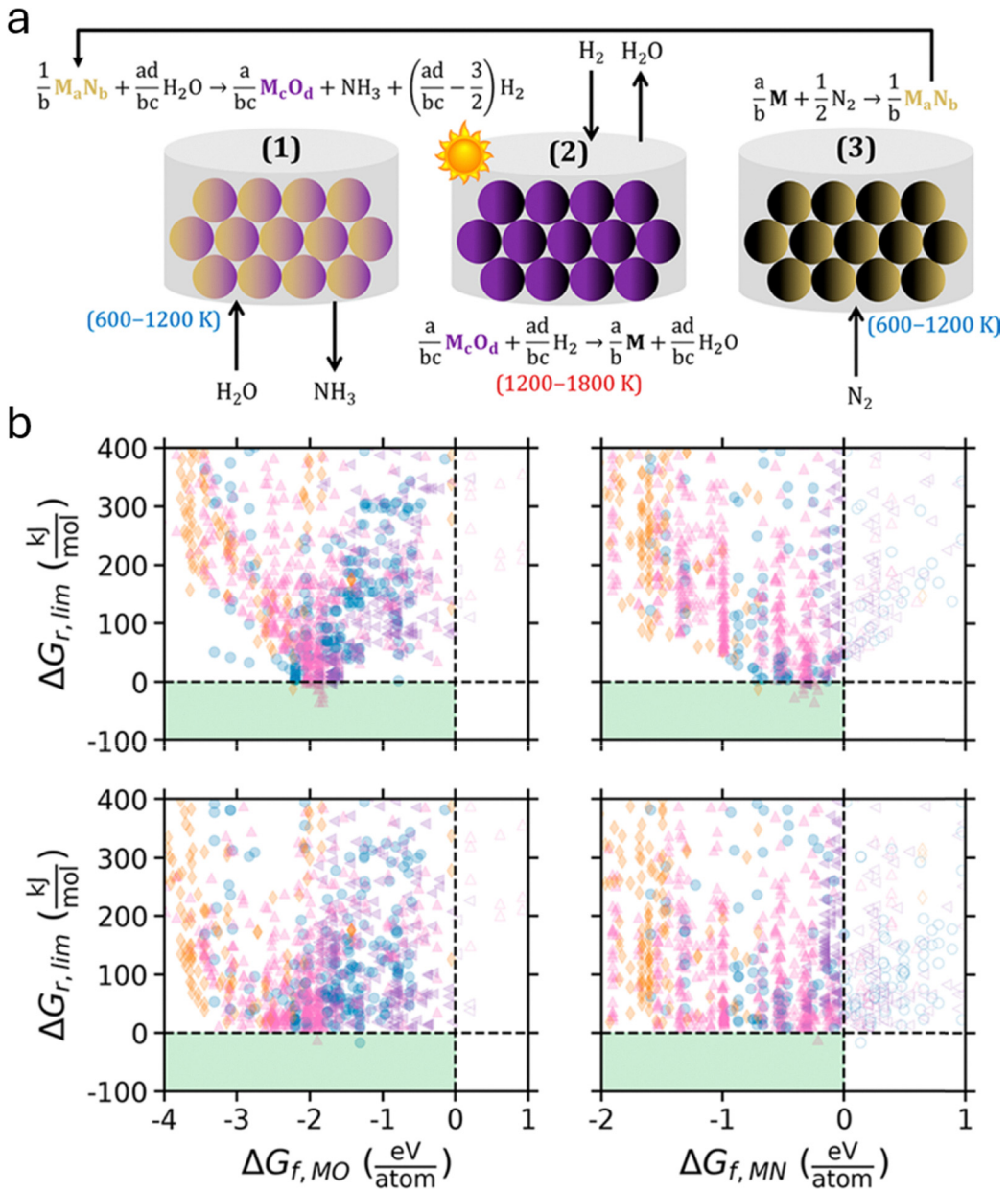

Fig. 7 (a) Solar thermochemical ammonia synthesis (STAS) reaction scheme. (b) Volcano dependence of STAS energetics. Limiting reaction plot for three-step STAS (top) and two-step STAS (bottom). The maximum allowable temperature swing is set to 600–1800 K. ΔG_f is reported at 0 K to present the target formation enthalpies for each reactant, which determines the minimum point of the volcano. This figure is adapted from ref. 30 with permission from American Chemical Society, copyright 2019.

2.3. Synergistic multielement carriers

The thermodynamic information for the mixed oxides generated from computational models, such as those presented in Section 2.1, can be quite useful to design and optimize oxide materials beyond redox-based chemical looping processes. In a recent study, Cai *et al.* addressed several inherent limitations of a CaO-based CO_2 sorbent in the context of sorption-enhanced reforming and gasification processes.[84–87] These limitations include: (1) the need for large temperature increases to drive the de-carbonation or calcination reaction; (2) deactivation over repeated carbonation–calcination cycles; and (3) limited sorbent operating temperature for the CO_2 uptake step, which limits the kinetics for gasification or reforming reactions.

To tackle these challenges, the authors proposed that perovskite-structured materials, which can readily incorporate alkali earth cations at the A-site and transition metal cations at the B-site, are among the mixed oxide options that meet the needed criteria.[70,88,89] Using the computed $Sr_xA_{1-x}Fe_yB_{1-y}O_{3-\delta}$ enthalpy and entropy values coupled with tabulated thermodynamic parameters for simple oxides, the thermodynamic feasibility for the oxide formation (synthesizability), sorption, and desorption reactions can be calculated based on the

following solid state reactions:

Synthesizability:

$$x\mathrm{SrO} + \frac{1-x}{m}\mathrm{A}_m\mathrm{O}_n + \frac{y}{2}\mathrm{Fe_2O_3} + \frac{1-y}{i}\mathrm{B}_i\mathrm{O}_j + z_1\mathrm{O_2} \rightarrow \mathrm{Sr}_x\mathrm{A}_{1-x}\mathrm{Fe}_y\mathrm{B}_{1-y}\mathrm{O}_{2.5} \quad (1)$$

Sorption reaction:

$$\mathrm{Sr}_x\mathrm{A}_{1-x}\mathrm{Fe}_y\mathrm{B}_{1-y}\mathrm{O}_{2.5} + \mathrm{CO_2} + z_2\mathrm{H_2} \rightarrow x\mathrm{SrCO_3} + \frac{1-x}{m}\mathrm{A}_m\mathrm{CO}_3 + \frac{y}{2}\mathrm{Fe_2O_3} + \frac{1-y}{i}\mathrm{B}_i\mathrm{O}_j + z_2\mathrm{H_2O} \quad (2)$$

Desorption reaction:

$$x\mathrm{SrCO_3} + \frac{1-x}{m}\mathrm{A}_m\mathrm{CO}_3 + \frac{y}{2}\mathrm{Fe_2O_3} + \frac{1-y}{i}\mathrm{B}_i\mathrm{O}_j + z_3\mathrm{O_2} \rightarrow \mathrm{Sr}_x\mathrm{A}_{1-x}\mathrm{Fe}_y\mathrm{B}_{1-y}\mathrm{O}_{2.5} + \mathrm{CO_2} \quad (3)$$

Using the procedure depicted in Fig. 8a, the authors assessed 1225 perovskite structures for their thermodynamic feasibility to reversibly and isothermally absorb and release CO_2. The aim was to identify materials that can achieve a high CO_2 sorption capacity without requiring the thermal swings needed for conventional sorbents. Through this screening, $SrMnO_{3-\delta}$ and related compounds were identified as promising candidates. These materials achieved CO_2 sorption capacities of up to 78% in TGA experiments, significantly surpassing the levels needed for practical applications (Fig. 8b). Their uniquely adaptable structure enables the reversible incorporation and release of lattice oxygen, which is essential for maintaining the redox cycle required for effective CO_2 capture and release.

Additionally, this study identified a correlation between thermodynamic parameters and sorption capacity, providing a useful descriptor for optimizing sorbents.[70] Among the screened candidates, $SrMnO_3$ demonstrated significant promise, particularly for biomass gasification and methane/biogas reforming, yielding green hydrogen and hydrogen-enriched syngas. The experimental results, summarized in Fig. 8b and c, validate the computational predictions and highlight the material's potential for practical applications.

3. Summary and outlook

The urgent need to mitigate global climate change demands transformative technologies that can decarbonize power generation and

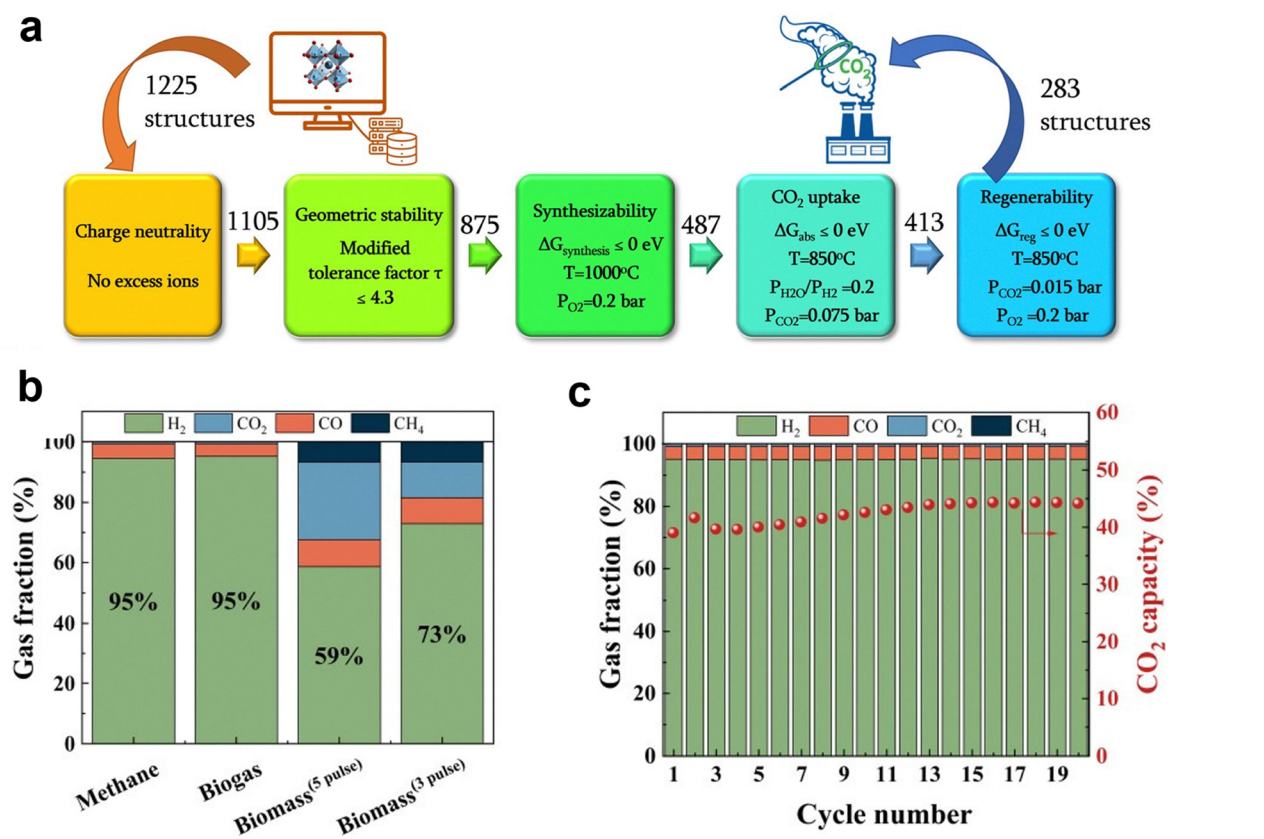

Fig. 8 (a) Computational screening workflow for iSERG sorbents. The values above each arrow represent the count of perovskite structures that successfully passed the preceding screening step. (b) Performance of the $SrMnO_3$ sorbent for isothermal gasification of various biomass feedstocks and reforming of methane and biogas. All the experiments were conducted isothermally at 850 °C; (c) conversion of biogas with a 2 : 1 ratio of CH_4 : CO_2. Reforming reaction is performed at 850 °C and a 2 : 1 steam to carbon ratio. This figure is reproduced from ref. 70 with permission from the Royal Society of Chemistry, copyright 2024.

heavy manufacturing. Chemical looping strategies, with their intrinsic ability to integrate chemical transformation, energy conversion, and simultaneous feedstock/product separation, offer unique opportunities to simplify industrial processes, improve energy efficiency, and lower CO_2 emissions. Realization of this potential hinges upon the discovery and optimization of high-performance carrier materials, *e.g.*, oxygen or nitrogen carriers, for these looping systems. Computational screening approaches, particularly high-throughput density functional theory (DFT) calculations combined with data-driven analysis, are now reshaping the development of these carrier materials for chemical looping beyond combustion. Even with simplifying assumptions (for example, modeling random distributions of dopants and focusing on equilibrium thermodynamics over kinetics), these methods have proven powerful in accelerating materials discovery. Indeed, they have uncovered new oxygen and nitrogen carrier compositions that would likely not have emerged from traditional trial-and-error experimentation.

However, current computational models still face important limitations. Table 1 summarizes a few key areas requiring focused development, along with the corresponding emerging solutions. Computational accuracy and realistic modeling assumptions remain critical bottlenecks. Mixed metal compounds present numerous possible cation distributions, yet current calculations struggle to account for potential cation ordering or defect clustering that may occur in real materials. The complexity intensifies with multi-valency transition metals, where defect and vacancy structures significantly impact the calculation results. Conventional DFT studies can only explore limited structural variants and disorder patterns, leading to substantial errors in entropy and free energy predictions. Additionally, commonly used Hubbard U parameters from general databases require system-specific calibration for accurate results.[90,91] Recent advances in system-specific benchmarking protocols and explicit defect ordering models show promise for addressing these limitations. Moving forward, continued advances in computational materials science will be pivotal for overcoming these challenges. In particular, expanding the availability of high-fidelity training data, *via* both more accurate theoretical calculations and high-throughput experiments, will improve machine learning models, making their predictions more robust and interpretable. Integrating emerging explainable artificial intelligence (XAI) techniques can further elucidate the fundamental structure–property relationships that govern reactive performance, guiding the rational and effective design of oxygen and nitrogen carrier materials.

We also note that material stability and synthesizability present intertwined challenges for CL carrier discovery. Most screening studies rely on thermodynamic criteria, such as the energy above hull (E_{hull}), which analyzes the thermodynamic stability of a material relative to other stable products from its constituents.[92] E_{hull} provides a straightforward way to evaluate structural stability. However, as mentioned above, defect and vacancy structures in the materials of interest can be highly complex and evolve dynamically during chemical looping cycles. Current DFT approaches can only sample limited structural configurations, leading to uncertainties in both enthalpic and entropic contributions to free energy calculations. Phonopy-based entropy calculations, while widely used, may not capture the full complexity of vibrational modes in disordered oxide systems. These computational limitations would compound when attempting to predict synthesizability, as kinetic barriers and metastable intermediate phases are often inadequately represented in equilibrium-based screening approaches.

Beyond thermodynamic stability, CL materials must maintain cyclic stability through reversible phase transitions and defect creation/annihilation processes under harsh operating conditions. The dynamic nature of these structural changes, such as ion migration, nucleation, and phase segregation, requires simulation methods that can capture both thermodynamic and kinetic effects across multiple length and time scales. Machine learning force fields (MLFFs) trained on high-fidelity DFT data offer a promising approach for modeling these phenomena in larger, more realistic systems. Kinetic Monte Carlo simulations excel at capturing rare events and long-timescale evolution, while phase field modeling and multiscale coupling approaches provide complementary insights into mesoscale structural evolution during chemical looping operation.

Target phase formation and reaction pathway determination historically relied on trial-and-error approaches. Traditional thermodynamic stability analysis using formation energies and convex hull methods provides the foundation for identifying potentially stable phases, but these equilibrium-based

Table 1 Challenges and solutions in high-throughput chemical looping carrier discovery

Challenges	Possible solutions/available tools	Ref.
Computational inaccuracy and realistic modeling assumptions	System-specific calibration and benchmarking; explicit defect/dopant ordering models; advanced or hybrid exchange–correlation functionals	90 and 91
Material stability during CL conditions	Machine learning force fields (MLFFs); kinetic Monte Carlo (KMC) simulations; phase field modeling; multiscale coupling approaches	95–98
Target phase formation and reaction pathway determination	Cellular automaton simulation frameworks; graph-based reaction network analysis; ML-predicted synthesis routes	93 and 94
Reaction simulation under CL conditions	Stochastic surface walking global optimization combined with global neural network potential, reaction mechanism generator	99–103
Standardized workflows and experimental validation	Digital twin frameworks; self-driving labs	104–107

approaches have inherent limitations. While convex hull analysis can predict the most thermodynamically favorable products, it cannot account for kinetic barriers that may prevent the formation of the predicted phases or lead to metastable intermediates during synthesis. To address these limitations, Persson's group integrated the convex hull concept and developed cellular automaton simulation frameworks that enable the prediction of time-dependent phase evolution during solid-state reactions.[93] They also developed graph-based reaction networks using path-finding algorithms that can suggest likely synthesis routes by mapping thermodynamic relationships between materials and identifying low-energy reaction pathways.[94] These integrated approaches provide systematic methods to identify viable synthesis recipes and predict both target phase formation and potential impurity phases that may compete during synthesis.

Reaction simulation under chemical looping conditions represents a critical frontier for mechanistic understanding. CL processes involve complex phase transition reactions at solid–solid and solid–gas interfaces, where detailed reaction mechanisms often are poorly understood. Stochastic surface walking global optimization combined with global neural network potentials offers a promising approach for exploring these complex reaction landscapes. This method has successfully revealed mechanistic insights into related catalytic systems, such as silver surface oxide formation during ethene epoxidation.[100] Additionally, the reaction mechanism generator (RMG)[102,103] and similar automated network generation tools show promise for identifying key elementary steps and reaction pathways in gas-phase and surface processes. A similar approach may be adopted/expanded to chemical looping reactions.

Lastly, current computational workflows lack standardization, making it difficult to systematically integrate experimental feedback to refine theoretical predictions and screening criteria. The emergence of self-driving laboratories could provide a powerful new paradigm for materials discovery. These autonomous research systems integrate automated synthesis, high-throughput characterization, and machine learning-driven decision-making into a closed-loop workflow. In such a system, computational models propose candidate materials; automated synthesis robots prepare and process those candidates; high-throughput experiments then test their properties; and machine learning algorithms analyze the results in real time to refine the models' predictions. Digital twin frameworks that mirror experimental conditions can further enhance this integration by providing virtual testbeds for optimization before physical synthesis. This combination of physics-based simulation, data-driven prediction, and autonomous experimentation can significantly reduce the time and cost associated with identifying optimal new redox materials.

By harnessing the synergy among advanced computation, data-driven modeling, and automated experimentation, we can envision an accelerated discovery pipeline for chemical looping materials. In this framework, high-throughput computational screening serves as an initial filter to map the vast chemical space of possible candidate compounds. Machine learning models then rank and prioritize these candidates through multi-objective optimization (balancing factors such as redox capacity, stability over cycling, productivity, and cost). Finally, autonomous laboratories rapidly synthesize and evaluate the top-ranked candidates, providing experimental feedback to continually refine the computational models and design criteria. Such an iterative, hybrid approach could reveal entirely new families of redox-active materials, optimize reactor operating conditions, and even guide the discovery of novel reaction pathways or mechanisms that would remain inaccessible with conventional trial-and-error methods. Ultimately, integrating advanced computation, data science, and autonomous experimentation holds great promise for transforming the landscape of chemical looping technology and significantly accelerating the development of the next generation of materials vital to global decarbonization.

Conflicts of interest

There are no conflicts to declare.

Data availability

No primary research results, software or code have been included, and no new data were generated as part of this perspective article.

Acknowledgements

This work was supported by the US National Science Foundation (2116724 and 2329857) and the U.S. Department of Energy (EE0008809, FE032355, and FE0032513).

References

1 J. Adanez, A. Abad, F. Garcia-Labiano, P. Gayan and L. F. de Diego, *Prog. Energy Combust. Sci.*, 2012, **38**, 215–282.
2 J. Adánez, A. Abad, T. Mendiara, P. Gayán, L. De Diego and F. García-Labiano, *Prog. Energy Combust. Sci.*, 2018, **65**, 6–66.
3 T. Mattisson, M. Keller, C. Linderholm, P. Moldenhauer, M. Ryden, H. Leion and A. Lyngfelt, *Fuel Process. Technol.*, 2018, **172**, 1–12.
4 T. Song and L. H. Shen, *Int. J. Greenhouse Gas Control.*, 2018, **76**, 92–110.
5 A. Lyngfelt, A. Brink, Ø. Langørgen, T. Mattisson, M. Rydén and C. Linderholm, *Int. J. Greenhouse Gas Control.*, 2019, **88**, 38–56.
6 S. Ramkumar, M. V. Iyer and L.-S. Fan, *Ind. Eng. Chem. Res.*, 2011, **50**, 1716–1729.
7 M. Vasilije and E. J. Anthony, *Environ. Sci. Technol.*, 2011, **45**, 10750–10756.

8 B. Arias, M. E. Diego, J. C. Abanades, M. Lorenzo, L. Diaz, D. Martínez, J. Alvarez and A. Sánchez-Biezma, *Int. J. Greenhouse Gas Control*, 2013, **18**, 237–245.
9 M. Zhao, J. Shi, X. Zhong, S. Tian, J. Blamey, J. Jiang and P. S. Fennell, *Energy Environ. Sci.*, 2014, **7**, 3291–3295.
10 J. Dou, E. Krzystowczyk, A. Mishra, X. B. Liu and F. X. Li, *ACS Sustainable Chem. Eng.*, 2018, **6**, 15528–15540.
11 E. Krzystowczyk, X. Wang, J. Dou, V. Haribal and F. Li, *Phys. Chem. Chem. Phys.*, 2020, **22**, 213–223.
12 R. Cai, J. Dou, E. Krzystowczyk, A. Richard and F. Li, *Chem. Eng. J.*, 2022, **429**, 132370.
13 X. Li, X. Sun, Q. Song, Z. Yang, H. Wang and Y. Duan, *Int. J. Hydrogen Energy*, 2022, **47**, 33619–33642.
14 L. Wei, Z. Pan, X. Shi, O. C. Esan, G. Li, H. Qi, Q. Wu and L. An, *iScience*, 2023, **26**, 108127.
15 J. T. Tran, K. J. Warren, S. A. Wilson, C. L. Muhich, C. B. Musgrave and A. W. Weimer, *WIREs Energy Environ.*, 2024, **13**, e528.
16 B. Chen, H. Kildahl, H. Yang, Y. Ding, L. Tong and L. Wang, *J. Energy Chem.*, 2024, **90**, 464–485.
17 S. Ghandehariun, M. A. Yekta and G. F. Naterer, *Int. J. Hydrogen Energy*, 2024, **96**, 1310–1327.
18 C. Liu, J. Park, H. A. De Santiago, B. Xu, W. Li, D. Zhang, L. Zhou, Y. Qi, J. Luo and X. Liu, *ACS Catal.*, 2024, **14**, 14974–15013.
19 Q. Wang, Y. Xuan, Z. Zhu, L. Teng, X. Liu and Y. Gao, *J. Mater. Chem. A*, 2025, **13**, 29558–29569.
20 R. Michalsky, P. H. Pfromm and A. Steinfeld, *Interface Focus*, 2015, **5**, 20140084.
21 W. B. Gao, J. P. Guo, P. K. Wang, Q. R. Wang, F. Chang, Q. J. Pei, W. J. Zhang, L. Liu and P. Chen, *Nat. Energy*, 2018, **3**, 1067–1075.
22 C. J. Bartel, J. R. Rumptz, A. W. Weimer, A. M. Holder and C. B. Musgrave, *ACS Appl. Mater. Interfaces*, 2019, **11**, 24850–24858.
23 S. Bhavsar, M. Najera, R. Solunke and G. Veser, *Catal. Today*, 2014, **228**, 96–105.
24 L. Zeng, Z. Cheng, J. A. Fan, L. S. Fan and J. L. Gong, *Nat. Rev. Chem.*, 2018, **2**, 349–364.
25 I. S. Metcalfe, B. Ray, C. Dejoie, W. Hu, C. de Leeuwe, C. Dueso, F. R. Garcia-Garcia, C. M. Mak, E. I. Papaioannou, C. R. Thompson and J. S. O. Evans, *Nat. Chem.*, 2019, **11**, 638–643.
26 Y. Gao, X. Wang, J. Liu, C. Huang, K. Zhao, Z. Zhao, X. Wang and F. Li, *Sci. Adv.*, 2020, **6**, eaaz9339.
27 X. Zhu, Q. Imtiaz, F. Donat, C. R. Muller and F. X. Li, *Energy Environ. Sci.*, 2020, **13**, 772–804.
28 D. Li, R. Xu, Z. Gu, X. Zhu, S. Qing and K. Li, *Energy Technol.*, 2020, **8**, 1900925.
29 Y. Gao, X. Wang, N. Corolla, T. Eldred, A. Bose, W. Gao and F. Li, *Sci. Adv.*, 2022, **8**, eabo7343.
30 C. J. Bartel, J. R. Rumptz, A. W. Weimer, A. M. Holder and C. B. Musgrave, *ACS Appl. Mater. Interfaces*, 2019, **11**, 24850–24858.
31 J. Fan, W. Li, S. Li and J. Yang, *Adv. Sci.*, 2022, **9**, 2202811.
32 R. J. Lee Pereira, I. S. Metcalfe and W. Hu, *Appl. Energy Combust. Sci*, 2023, **16**, 100226.
33 M. B. Gawande, R. K. Pandey and R. V. Jayaram, *Catal. Sci. Technol.*, 2012, **2**, 1113–1125.
34 N. Kumar, Sauraj and N. C. Joshi, *Solid Base Catalysts*, 2024, DOI: **10.1002/9783527846719.ch10**, pp. 279–315.
35 T. Song, E. U. Hartge, S. Heinrich, L. H. Shen and J. Werther, *Int. J. Greenhouse Gas Control*, 2018, **70**, 22–31.
36 H. B. Zhao and J. X. Wang, *Combust. Flame*, 2018, **191**, 9–18.
37 I. Gogolev, C. Linderholm, D. Gall, M. Schmitz, T. Mattisson, J. B. C. Pettersson and A. Lyngfelt, *Int. J. Greenhouse Gas Control*, 2019, **88**, 371–382.
38 H. Zhao, X. Tian, J. Ma, X. Chen, M. Su, C. Zheng and Y. Wang, *Energy Fuels*, 2020, **34**, 6696–6734.
39 Z. H. Gu, L. Zhang, C. Q. Lu, S. Qing and K. Z. Li, *Appl. Energy*, 2020, **277**, 115590.
40 L. Liu, Z. S. Li, L. J. Wang, Z. H. Zhao, Y. Li and N. S. Cai, *Ind. Eng. Chem. Res.*, 2020, **59**, 7238–7246.
41 L. Liu, Z. S. Li, S. J. Wu, D. Li and N. S. Cai, *Fuel Process. Technol.*, 2021, **213**, 106711.
42 L. Liu, Z. S. Li, Z. A. Li, Y. Larring and N. S. Cai, *Chem. Eng. J.*, 2021, **417**, 128054.
43 J. Liu, S. Yusuf, D. Jackson, W. Martin, D. Chacko, K. Vogt-Lowell, L. Neal and F. Li, *Appl. Catal., A*, 2022, **646**, 118869.
44 A. Lyngfelt, B. Leckner and T. Mattisson, *Chem. Eng. Sci.*, 2001, **56**, 3101–3113.
45 J. Vieten, B. Bulfin, F. Call, M. Lange, M. Schmücker, A. Francke, M. Roeb and C. Sattler, *J. Mater. Chem. A*, 2016, **4**, 13652–13659.
46 H. C. Wu and Y. S. Lin, *Ind. Eng. Chem. Res.*, 2017, **56**, 6057–6064.
47 E. Krzystowczyk, X. J. Wang, J. Dou, V. Haribal and F. X. Li, *Phys. Chem. Chem. Phys.*, 2020, **22**, 8924–8932.
48 R. H. Görke, E. J. Marek, F. Donat and S. A. Scott, *Int. J. Greenhouse Gas Control*, 2020, **94**, 102891.
49 E. Krzystowczyk, V. Haribal, J. Dou and F. X. Li, *ACS Sustainable Chem. Eng.*, 2021, **9**, 12185–12195.
50 J. Dou, E. Krzystowczyk, X. J. Wang, A. R. Richard, T. Robbins and F. X. Li, *J. Phys. Energy*, 2020, **2**, 025007.
51 Q. H. Zheng, M. Lail, S. J. Zhou and C. C. Chun, *ChemSusChem*, 2019, **12**, 2598–2604.
52 C.-C. Cormos, *Energy*, 2020, **191**, 116579.
53 B. Bulfin, J. Lapp, S. Richter, D. Gubàn, J. Vieten, S. Brendelberger, M. Roeb and C. Sattler, *Chem. Eng. Sci.*, 2019, **203**, 68–75.
54 M. Xu, H. C. Wu, Y. S. Lin and S. G. Deng, *Chem. Eng. J.*, 2018, **354**, 62–74.
55 C. Tagliaferri, R. Görke, S. Scott, J. Dennis and P. Lettieri, *Chem. Eng. Res. Design*, 2018, **131**, 686–698.
56 A. Moran and O. Talu, *Ind. Eng. Chem. Res.*, 2018, **57**, 11981–11987.
57 L. M. Hou, Q. B. Yu, T. Wang, K. Wang, Q. Qin and Z. F. Qi, *Korean J. Chem. Eng.*, 2018, **35**, 626–636.
58 L. S. Fan, L. Zeng, W. L. Wang and S. W. Luo, *Energy Environ. Sci.*, 2012, **5**, 7254–7280.
59 Z. Cheng, D. S. Baser, S. G. Nadgouda, L. Qin, J. A. Fan and L. S. Fan, *ACS Energy Lett.*, 2018, **3**, 1730–1736.
60 D. S. Baser, Z. Cheng, J. A. Fan and L. S. Fan, *ACS Sustainable Chem. Eng.*, 2021, **9**, 2651–2660.

61 H. M. Gu, L. H. Shen, J. Xiao, S. W. Zhang and T. Song, *Energy Fuels*, 2011, **25**, 446–455.
62 R. B. Dudek, X. Tian, M. Blivin, L. M. Neal, H. B. Zhao and F. X. Li, *Appl. Catal., B*, 2019, **246**, 30–40.
63 W. X. Ding, K. Zhao, S. C. Jiang, Z. L. Zhao, Y. Cao and F. He, *Appl. Catal., A*, 2021, **609**, 117910.
64 F. Donat, A. Kierzkowska and C. R. Muller, *Energy Fuels*, 2022, **36**, 9780–9784.
65 H. Gu, Y. Gao, S. Iftikhar and F. Li, *J. Mater. Chem. A*, 2022, **10**, 3077–3085.
66 J. Liu and F. Li, *Chem. Commun.*, 2023, **59**, 10–28.
67 C. Y. Lau, M. T. Dunstan, W. Hu, C. P. Grey and S. A. Scott, *Energy Environ. Sci.*, 2017, **10**, 818–831.
68 X. Tian, C. H. Zheng and H. B. Zhao, *Appl. Catal., B*, 2022, **303**, 120894.
69 A. Ramazani, B. A. Duell, E. J. Popczun, S. Natesakhawat, T. Nandi, J. W. Lekse and Y. Duan, *Cell Rep. Phys. Sci.*, 2024, **5**, 101797.
70 R. Cai, K. Yang, X. Wang, M. Rukh, A. S. Bosari, E. Giavedoni, A. Pierce, L. Brody, W. Tang, P. R. Westmoreland and F. Li, *Energy Environ. Sci.*, 2024, **17**, 6279–6290.
71 S. Iftikhar, W. Martin, Y. F. Gao, X. B. Yu, I. W. Wang, Z. L. Wu and F. X. Li, *Catal. Today*, 2023, **416**, 113854.
72 J. Dou, J. Funderburg, K. Yang, J. Liu, D. Chacko, K. Zhang, A. P. Harvey, V. P. Haribal, S. J. Zhou and F. Li, *ACS Catal.*, 2023, **13**, 213–223.
73 R. Cai, H. Bektas, X. Wang, K. McClintock, L. Teague, K. Yang and F. Li, *Adv. Energy Mater.*, 2023, **13**, 2203833.
74 X. Wang, Y. Gao, E. Krzystowczyk, S. Iftikhar, J. Dou, R. Cai, H. Wang, C. Ruan, S. Ye and F. Li, *Energy Environ. Sci.*, 2022, **15**, 1512–1528.
75 N. R. Singstock, C. J. Bartel, A. M. Holder and C. B. Musgrave, *Adv. Energy Mater.*, 2020, **10**, 2000685.
76 P. Tolstova, R. Ahmad, A. C. Sepulveda and L. Cavallo, *Small*, 2024, 2407601.
77 K. Zhao, F. He, Z. Huang, G. Wei, A. Zheng, H. Li and Z. Zhao, *Appl. Energy*, 2016, **168**, 193–203.
78 F. He, J. Chen, S. Liu, Z. Huang, G. Wei, G. Wang, Y. Cao and K. Zhao, *Int. J. Hydrogen Energy*, 2019, **44**, 10265–10276.
79 A. A. Emery, J. E. Saal, S. Kirklin, V. I. Hegde and C. Wolverton, *Chem. Mater.*, 2016, **28**, 5621–5634.
80 H. Bektas, R. Cai, L. Brody and F. Li, *Energy Fuels*, 2024, **38**, 11107–11118.
81 D. Notter, T. Elias Abi-Ramia Silva, M. E. Gálvez, B. Bulfin and A. Steinfeld, *Mater. Horiz.*, 2024, **11**, 4054–4063.
82 J. Guo and P. Chen, *Acc. Chem. Res.*, 2021, **54**, 2434–2444.
83 L. Zhou, X. Li, Q. Li, A. Kalu, C. Liu, X. Liu and W. Li, *ACS Catal.*, 2023, **13**, 15087–15106.
84 D. Kang, M. Lee, H. S. Lim and J. W. Lee, *Fuel*, 2018, **215**, 787–798.
85 M. T. Dunstan, F. Donat, A. H. Bork, C. P. Grey and C. R. Müller, *Chem. Rev.*, 2021, **121**, 12681–12745.
86 Y. Kim, H. S. Lim, H. S. Kim, M. Lee, J. W. Lee and D. Kang, *J. CO2 Util.*, 2022, **63**, 102139.
87 R. Chang, X. Wu, O. Cheung and W. Liu, *J. Mater. Chem. A*, 2022, **10**, 1682–1705.
88 M. Rukh, R. Cai, L. Brody and F. Li, *Chem. Eng. J.*, 2024, **501**, 157545.
89 L. Brody, R. Cai, A. Thornton, J. Liu, H. Yu and F. Li, *ACS Sustainable Chem. Eng.*, 2022, **10**, 6434–6445.
90 M. K. Horton, P. Huck, R. X. Yang, J. M. Munro, S. Dwaraknath, A. M. Ganose, R. S. Kingsbury, M. Wen, J. X. Shen, T. S. Mathis, A. D. Kaplan, K. Berket, J. Riebesell, J. George, A. S. Rosen, E. W. C. Spotte-Smith, M. J. McDermott, O. A. Cohen, A. Dunn, M. C. Kuner, G.-M. Rignanese, G. Petretto, D. Waroquiers, S. M. Griffin, J. B. Neaton, D. C. Chrzan, M. Asta, G. Hautier, S. Cholia, G. Ceder, S. P. Ong, A. Jain and K. A. Persson, *Nat. Mater.*, 2025, **24**, 1522–1532.
91 A. Jain, G. Hautier, S. P. Ong, C. J. Moore, C. C. Fischer, K. A. Persson and G. Ceder, *Phys. Rev. B*, 2011, **84**, 045115.
92 A. Jain, S. P. Ong, G. Hautier, W. Chen, W. D. Richards, S. Dacek, S. Cholia, D. Gunter, D. Skinner, G. Ceder and K. A. Persson, *APL Mater.*, 2013, **1**, 011002.
93 M. C. Gallant, M. J. McDermott, B. Li and K. A. Persson, *Chem. Mater.*, 2025, **37**, 210–223.
94 M. J. McDermott, S. S. Dwaraknath and K. A. Persson, *Nat. Commun.*, 2021, **12**, 3097.
95 C. R. Salazar, A. K. Ammothum Kandy, J. Furstoss, Q. Gromoff, J. Goniakowski and J. Lam, *Npj Comput. Mater.*, 2024, **10**, 199.
96 T. Martynec, C. Karapanagiotis, S. H. L. Klapp and S. Kowarik, *Commun. Mater.*, 2021, **2**, 90.
97 M. Yang, L. Wang and W. Yan, *Npj Comput. Mater.*, 2021, **7**, 56.
98 L. Zhang, W. Ren, A. Samanta and Q. Du, *Npj Comput. Mater.*, 2016, **2**, 16003.
99 X.-T. Xie, Z.-X. Yang, D. Chen, Y.-F. Shi, P.-L. Kang, S. Ma, Y.-F. Li, C. Shang and Z.-P. Liu, *Precis. Chem.*, 2024, **2**, 612–627.
100 D. Chen, L. Chen, Q.-C. Zhao, Z.-X. Yang, C. Shang and Z.-P. Liu, *Nat. Catal.*, 2024, **7**, 536–545.
101 X.-T. Xie, T. Guan, Z.-X. Yang, C. Shang and Z.-P. Liu, *J. Chem. Theory Comput.*, 2025, **21**, 3576–3586.
102 M. S. Johnson, X. Dong, A. Grinberg Dana, Y. Chung, D. Farina Jr, R. J. Gillis, M. Liu, N. W. Yee, K. Blondal, E. Mazeau, C. A. Grambow, A. M. Payne, K. A. Spiekermann, H.-W. Pang, C. F. Goldsmith, R. H. West and W. H. Green, *J. Chem. Inf. Model.*, 2022, **62**, 4906–4915.
103 M. Liu, A. Grinberg Dana, M. S. Johnson, M. J. Goldman, A. Jocher, A. M. Payne, C. A. Grambow, K. Han, N. W. Yee, E. J. Mazeau, K. Blondal, R. H. West, C. F. Goldsmith and W. H. Green, *J. Chem. Inf. Model.*, 2021, **61**, 2686–2696.
104 Y. Song, Z. Chen, Y. Zhou, D. Fang, Y. Lu, R. Xiao and D. Zeng, *Int. J. Hydrogen Energy*, 2024, **61**, 568–577.
105 G. Tom, S. P. Schmid, S. G. Baird, Y. Cao, K. Darvish, H. Hao, S. Lo, S. Pablo-García, E. M. Rajaonson, M. Skreta, N. Yoshikawa, S. Corapi, G. D. Akkoc, F. Strieth-Kalthoff, M. Seifrid and A. Aspuru-Guzik, *Chem. Rev.*, 2024, **124**, 9633–9732.
106 M. Sim, M. G. Vakili, F. Strieth-Kalthoff, H. Hao, R. J. Hickman, S. Miret, S. Pablo-García and A. Aspuru-Guzik, *Matter*, 2024, **7**, 2959–2977.
107 S. X. Leong, C. E. Griesbach, R. Zhang, K. Darvish, Y. Zhao, A. Mandal, Y. Zou, H. Hao, V. Bernales and A. Aspuru-Guzik, *Nat. Rev. Chem.*, 2025, **9**, 707–722.